Three-body-potential contribution to the structure of krypton gas

Albert Teitsma and P. A. Egelstaff

Physics Department, University of Guelph, Guelph, Ontario N1G 2W1, Canada

The virial expansion for the inverse structure factor of a gas is known to involve coefficients which are a function of q and T, and whose $q \to 0$ limits are the usual pressure virial coefficients. The authors have made careful measurements of the structure factor of krypton gas using improved neutron-diffraction techniques at 15 densities between 0.25 and 6.19×10^{27} atoms/m^3 at $T = 297$ K. The methods used are described, and the experimental errors are analyzed and found to be less than 1%. These data are compared to virial-expansion calculations based on the Barker *et al.* pair potential, to extract the first coefficient depending on the triplet potential. Some difference is found between this result and that predicted by the long-range triple-dipole (Axilrod-Teller) term.

I. INTRODUCTION AND THEORY

It has been known for many years that the coefficients of the virial expansion for the pressure of the noble gases must be discussed in terms of both pair and higher-order forces. For example, this virial series can be written as

$$P/kT = \lim_{q \to 0} \{ \rho + \rho^2 B(q, T)$$
$$+ \rho^3 [C_1(q, T) + C_2(q, T)] + O(\rho^4) \},$$

$$(1)$$

where P is the pressure, k is Boltzmann's constant, T is the temperature, ρ is the density, and

$$B(q, T) = -\tfrac{1}{2} \int f(r) e^{i\vec{q} \cdot \vec{r}} d\vec{r},$$

$$C_1(q, T) = -\tfrac{1}{3} \int \int f(r) f(s) f(|\vec{r} - \vec{s}|) e^{i\vec{q} \cdot \vec{r}} d\vec{r} d\vec{s},$$

$$C_2(q, T) = -\tfrac{1}{3} \int \int [f(r) + 1][f(s) + 1][f(|\vec{r} - \vec{s}|) + 1]$$
$$\times (e^{-\beta u_3(\vec{r}, \vec{s})} - 1) e^{i\vec{q} \cdot \vec{r}} d\vec{r} d\vec{s},$$

where $\vec{r}$ is the displacement between a given pair of atoms, $\vec{s}$ is the displacement between one of these atoms and a third atom, $f(r) = e^{-\beta u_2(r)} - 1$, β is $1/kT$, u_2 and u_3 are the pair and triplet potentials, respectively, and $\vec{q}$ is the wave vector.

It has been found in PVT experiments that the term $C_2(q = 0)$, which is the first term dependent on the triplet potential, is significant. However, it is not widely appreciated that for two special state points this term can have a very large effect. These are the critical points for the real system or the pair system [i.e., a fluid of atoms interacting with the potential $u_2(r)$ alone]. It is easy to see that, because the compressibility is infinite at a critical point, the difference between com-

pressibilities of the two systems can be infinite. As we will discuss later, the pair system has a higher critical temperature than the real system. Thus at the critical density and near to but above the critical temperature of the *pair* system there will be very large differences between the compressibilities of the two systems. In contrast at the critical temperature of the *real* system the pair system will exist in two phases, since this is below its critical temperature.

While a great deal of information has been extracted for many years from Eq. (1), it would be advantageous if the r or, equivalently, the q dependence of the functions B and C could be obtained. This can be done by considering the virial series[1] for the pair distribution function $g(r)$:

$$g(r) = f(r) + 1 + \rho [f(r) + 1]$$

$$\times \left(\int f(\vec{s}) f(|\vec{r} - \vec{s}|) d\vec{s} + \int [f(\vec{s}) + 1] \right.$$

$$\left. \times [f(|\vec{r} - \vec{s}|) + 1](e^{-\beta u_3(\vec{r}, \vec{s})} - 1) d\vec{s} \right) + O(\rho^2).$$

$$(2)$$

Its Fourier transform gives the structure factor

$$S(q) = 1 + \rho \int [g(r) - 1] e^{i\vec{q} \cdot \vec{r}} dr,$$

$$(3)$$

and the direct correlation function, $c(q)$ $= [1 - S^{-1}(q)]/\rho$ is given in terms of B and C by

$$c(q) = -2B(q, T) - 3\rho [C_1(q, T) + C_2(q, T)] + O(\rho^2),$$

$$(4)$$

as can be seen by deriving (4) from (2) and comparing to the expressions for B and C given earlier. This expression differs from the corresponding expression for $[S(q) - 1]/\rho$ by the term $4\rho B^2(q, T)$. Also, the derivative of (1) with respect to ρ is $1 - \rho c(q \to 0)$, and thus we get the usual ex-

pression $S(0) = kT\rho\chi_T$, where χ_T is the isothermal compressibility. Finally $C_2(q, T)$ may be obtained from (4) by

$$C_2(q, T) = (1/3\rho)[c(q)_{pair} - c(q)_{expt}] + O(\rho) , \quad (5)$$

where $c(q)_{pair}$ is a direct correlation function calculated from the pair potential alone.

Pair potentials for krypton have been obtained by a number of authors[2,3] using reliable data, and so $u_2(r)$ is quite well known and has a well depth ϵ/k of 202 ± 1 K. We would like to know the critical temperature for a hypothetical fluid whose atoms interact with $u_2(r)$ alone. An effective potential, such as the Lennard-Jones, can be fitted to a significant body of data, and it is found that the well depth for this case is ~170 K. The first four virial coefficients of the pressure of a Lennard-Jones fluid with $\epsilon/k = 170$ K and of a hypothetical pair fluid with the same well depth are roughly the same, and so we assume their critical temperatures are nearly the same. In addition, the critical temperature for the Lennard-Jones system[4] with $\epsilon = 170$ K is ~230 K compared to 210 K for real krypton. We take the average of these (220 K) to be, approximately, the critical point of a hypothetical pair fluid with ϵ ~170 K. The ratio of well depths of these hypothetical pair fluids (i.e., 202/170) will be approximately the ratio of T_c's, and therefore we estimate T_c for the pair system with $\epsilon/k = 200$ K to be ~260 K. In order to be above this estimate and for obvious convenience, we have worked at approximately 297 K.

The functions $S(q)$ and $c(q)$ can be determined through neutron scattering experiments. Ideally these experiments measure a scattered intensity I proportional to $S(q)$, but in practice the scattering contains an incoherent component, so that at best one has

$$I \propto \sigma^{coh}[S(q) - 1] + \sigma^{tot} , \quad (6)$$

where σ^{coh} and σ^{tot} are the bound-atom coherent and the total scattering cross sections. In addition, one must correct for the inelasticity of the scattering, absorption of neutrons by the sample and container, multiple scattering, and electronic scattering. To obtain data which can be used in Eqs. (4) or (5), a high precision is required. Because the density must be small, the maximum absolute value of $S(q) - 1$, except at small q, will be about 0.2, and so its determination will require the differential cross section to be measured with a precision of better than 1%.

An experiment of this type will be sensitive to the form of potential about the minimum (from the repulsive part of the potential to about one atomic diameter beyond the minimum) at low densities; its sensitivity to other parts of $u_2(r)$ is not high.

Since $C_2(q)$ includes three-body effects, our experiment will be sensitive to $u_3(\vec{r}, \vec{s})$ in the same range of r, over which it is not well known. Thus a careful quantitative study of $S(q)$ for krypton gas is worthwhile for extracting $C_2(q)$, given $B(q)$.

This approach may be contrasted with that of Karnicky et al.,[5] who have measured three states of argon at 173 K and densities between 2.0 and 4.7 on our scale. They converted their $S(q)$ data to an effective pair potential, using an approximate series (Percus-Yevick) in place of Eq. (2) and the Axilrod-Teller potential for the three-body term. In contrast, we measure more states and assume that the two-body potential is well known, so that we can use Eq. (5) to discuss many-body effects and particularly the three-body term.

Measurements of $S(q)$ for krypton gas along the room-temperature isotherm were made for densities between 0.25×10^{27} and 6.2×10^{27} atoms/m^3. This range of densities was chosen to extend from the lowest value at which we felt useful data could be obtained to a value just above ρ_c. (For convenience, the units and exponent of the density will not be written out explicitly throughout the rest of this paper; for example, the above two densities will be referred to as 0.25 and 6.2.) Section II describes the experimental methods and Secs. III and IV the analysis of the results to find $S(q)$. Then we compare our results to theoretical predictions and extract $C_2(q)$ from the data by assuming that the pair potential for krypton is well known.

II. NEUTRON-DIFFRACTION EXPERIMENT

A. Spectrometer

The neutron diffractometer used for this experiment is described by Egelstaff et al.[6]: it was designed for gas-diffraction experiments and is installed at the NRU reactor at Chalk River Nuclear Laboratories. The spectrometer uses double monochromation to provide a 2.39-Å neutron beam with a 0.6° FWHM spread at the sample position. A graphite filter is placed between the sample and the monochromator to reduce the higher-order contamination (to ~0.3% for second order). The overall electronic stability is such that data can be collected with a statistical precision of 0.1%, and angles are reproducible to better than 0.05°. Two fission chambers monitored the primary beam before and after scattering. Scattered neutrons were detected by ^{3}He counters of two types: "rectangular" detectors (95% efficient at 2.4Å) 3.8 cm wide and 36 cm high, and cylindrical detectors (75% efficient) 2.5 cm in diameter and 41 cm high. These detectors were located at a (horizontal) radius of 216 cm from the sample and were sur-

rounded by two massive neutron shields. Two cy-
lindrical detectors, the detection length of which
had been masked down to 10 cm for use at small
scattering angles, were located along with six
rectangular detectors (bank I) in the first shield.
The second shield contained eight pairs of cylin-
drical detectors (bank II). These shields were
mounted on a carriage which moved in 0.5° steps,
resulting in a range of scattering angles of
~10–109°. This provided a range $0.2 \leqslant q \leqslant 4.3 Å^{-1}$,
which covers the significant part of $S(q) - 1$ for
noble gases.

B. Samples

All samples were mounted at the center of a 46
cm diameter rotatable chamber filled with argon.
Two cylindrical pressure vessels[7] (of wall thick-
nesses 3.2 and 2.4 mm) were made from aluminum
alloy 6061-T6 and were pressure tested to 300 and
150 atm, respectively, without significant changes
in diameter. The smaller vessel (vessel I, 3.49
cm i.d.) was used for the density range 2.88–6.19
and the larger vessel (vessel II, 6.99 cm i.d.) was
used for the density range 0.25–2.88. Gadolinium-
oxide–covered cylinders inside the vessels limited
the sample length to 7.62 cm.

Krypton was transferred between the storage
bottle and pressure vessels by the cryopump gas-
handling system shown schematically in Fig. 1.
The method consisted of condensing the krypton
from the storage bottle into the cryopump vessel,
which was held at liquid-nitrogen temperature;
by subsequently raising the temperature of the
cryopump vessel (with the appropriate valves
opened or closed) krypton was forced into the pres-
sure vessel. These steps were repeated until the

FIG. 1. Schematic layout of the krypton-gas-handling
system.

desired density was reached. Pressures were
measured with a Matheson precision 0–3000 psi
test gauge; densities were calculated from the
measured pressure using the PVT data[8] for kryp-
ton. The temperature was 297 K and was stable
to ±1 K. At the end of the experiment the gas was
analyzed by Matheson of Canada Ltd., with the
following results: oxygen, 10 ppm by weight; hy-
drogen, <10 ppm; nitrogen, 145 ppm; argon, 90
ppm; xenon, 1640 ppm.

Vanadium, which is an almost isotropic scatter-
er, was used to calibrate the scattered intensity
and to check for spurious instrumental fluctuations.
The principal calibration sample consisted of a
$0.0264 \times 15.3 \times 45.7$-$cm^3$ vanadium sheet (mass 110
g) rolled into a 3.5-cm-diam × 15.3-cm-high spiral,
and a secondary calibration sample was made of
seven pieces of $10.2 \times 7.6 \times 0.026$ cm^3 of vanadium
sheet rolled into a 6.8-cm-diam × 7.6-cm-high
spiral. Cadmium screening reduced the height of
the first spiral to 7.6 cm and that of the second
spiral to 7.0 cm.

A cadmium tube (15.2 cm diam and 0.07-cm
wall) surrounded all samples during the experi-
ment. A 2.5-cm-wide × 7-cm-high opening cut into
this tube defined the size and location of the pri-
mary beam for vessel I; for vessel II the opening
was widened to 5.0×5.0 cm^2. A second opening al-
lowed for the detection of scattered neutrons over
the angular range 0–100°. Cadmium disks (0.07
cm thick and 15.2 cm diam) were spaced 8 cm
apart on the vessel above and below the sample
volume. Data were taken for angles greater than
6° with this beam size. For lower angles the
masked-down counters were used and the beam
for vessel I was 2.5×2.5 cm^2 and for vessel II
2.4×5.0 cm^2, and data were used down to 3 and 4°,
respectively.

C. Experimental measurements

The main experiment consisted of measuring the
scattered intensities for a given number of monitor
counts from the krypton plus its container. At the
time of this experiment the electronic equipment
allowed data collection from only five detectors at
a time. Thus the scattered intensity at each den-
sity was measured in a "small-angle" run using
the two masked-down counters plus three rectang-
ular detectors from bank I, an "intermediate-an-
gle" run covering the scattering range ~6°–~60°
using five of the rectangular bank I detectors for
vessel I (or three for vessel II), and a "large-
angle" run covering the scattering angles from
~50° to ~100° using five of the bank II detectors.
Cadmium sheets restricted the opening of the de-
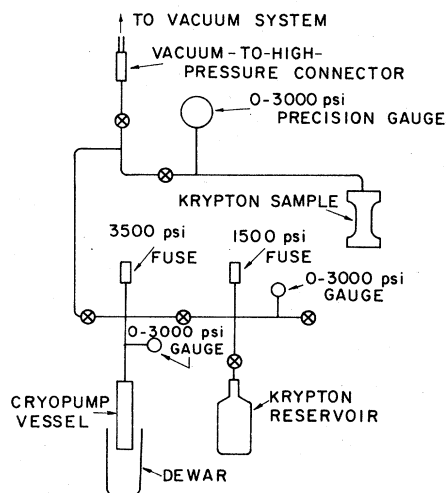tector shields, so that only the detectors in use

TABLE I. Listing of $S(q)$ for the 17 experiments (all data shown have been calibrated as described in Sec. IV. Densities are shown at the head of each column.

Q	0.253	0.258	0.520	0.799	1.517	1.964	2.425	2.883	2.884	3.160	3.474	3.817	4.216	4.66	5.15	5.65	6.19
0.0	1.042	1.044	1.088	1.140	1.269	1.348	1.425	1.495	1.483	1.521	1.560	1.582	1.601	1.594	1.540	1.490	1.419
0.2	1.025	1.027	1.059	1.088	1.161	1.193	1.222	1.198	1.165	1.157	1.144	1.148	1.118	1.091	1.015	0.945	0.900
0.25	1.019	1.022	1.048	1.069	1.123	1.140	1.155	1.108	1.072	1.062	1.049	1.045	1.012	0.975	0.920	0.847	0.806
0.3	1.012	1.017	1.035	1.047	1.085	1.087	1.090	1.034	0.999	0.986	0.973	0.945	0.927	0.879	0.835	0.776	0.731
0.35	1.006	1.011	1.022	1.027	1.046	1.032	1.020	0.972	0.936	0.924	0.909	0.885	0.853	0.809	0.769	0.718	0.672
0.4	1.000	1.003	1.010	1.006	1.009	0.985	0.961	0.920	0.886	0.870	0.856	0.827	0.797	0.753	0.720	0.667	0.624
0.45	0.995	0.997	0.998	0.988	0.971	0.942	0.913	0.872	0.849	0.828	0.810	0.783	0.752	0.712	0.677	0.627	0.587
0.5	0.992	0.991	0.989	0.970	0.937	0.905	0.869	0.831	0.811	0.796	0.771	0.748	0.714	0.678	0.644	0.599	0.557
0.55	0.989	0.984	0.980	0.952	0.908	0.879	0.839	0.802	0.786	0.768	0.743	0.720	0.688	0.650	0.614	0.572	0.537
0.6	0.986	0.980	0.973	0.938	0.888	0.857	0.815	0.779	0.764	0.747	0.723	0.699	0.668	0.629	0.599	0.557	0.521
0.65	0.984	0.973	0.967	0.927	0.873	0.840	0.800	0.764	0.753	0.735	0.708	0.687	0.658	0.621	0.589	0.549	0.513
0.7	0.982	0.971	0.963	0.921	0.865	0.829	0.792	0.755	0.747	0.728	0.702	0.682	0.650	0.618	0.586	0.546	0.511
0.75	0.981	0.971	0.960	0.918	0.859	0.824	0.789	0.750	0.745	0.727	0.701	0.680	0.647	0.619	0.587	0.547	0.515
0.8	0.980	0.970	0.959	0.919	0.858	0.823	0.789	0.748	0.745	0.729	0.705	0.683	0.649	0.624	0.592	0.556	0.521
0.85	0.980	0.970	0.959	0.923	0.860	0.826	0.793	0.752	0.751	0.736	0.712	0.690	0.657	0.632	0.605	0.564	0.535
0.9	0.983	0.971	0.962	0.928	0.865	0.834	0.800	0.759	0.760	0.747	0.724	0.702	0.669	0.645	0.618	0.578	0.551
0.95	0.985	0.972	0.965	0.934	0.874	0.844	0.811	0.773	0.774	0.761	0.738	0.717	0.687	0.662	0.636	0.599	0.570
1.0	0.987	0.975	0.970	0.940	0.885	0.855	0.823	0.789	0.792	0.780	0.756	0.736	0.709	0.683	0.657	0.620	0.592
1.05	0.990	0.978	0.975	0.948	0.897	0.869	0.840	0.808	0.815	0.800	0.778	0.760	0.733	0.707	0.683	0.647	0.623
1.1	0.992	0.982	0.980	0.956	0.911	0.886	0.861	0.829	0.839	0.822	0.802	0.789	0.763	0.738	0.715	0.680	0.658
1.15	0.994	0.985	0.984	0.964	0.926	0.904	0.884	0.854	0.863	0.849	0.831	0.819	0.796	0.774	0.750	0.719	0.689
1.2	0.996	0.989	0.989	0.972	0.941	0.922	0.906	0.880	0.890	0.880	0.860	0.854	0.830	0.815	0.787	0.761	0.740
1.25	0.998	0.993	0.994	0.981	0.956	0.942	0.928	0.908	0.918	0.911	0.894	0.891	0.868	0.856	0.830	0.809	0.789
1.3	1.000	0.996	0.999	0.989	0.970	0.962	0.953	0.936	0.947	0.941	0.930	0.927	0.907	0.897	0.877	0.858	0.842
1.35	1.002	0.999	1.004	0.997	0.985	0.983	0.976	0.966	0.975	0.972	0.964	0.963	0.948	0.941	0.928	0.909	0.896
1.4	1.003	1.002	1.008	1.005	1.000	1.001	0.998	0.994	1.004	1.003	0.997	0.999	0.990	0.985	0.977	0.960	0.956
1.45	1.005	1.004	1.011	1.013	1.013	1.018	1.019	1.020	1.031	1.032	1.027	1.033	1.028	1.027	1.025	1.011	1.013
1.5	1.006	1.007	1.014	1.021	1.026	1.034	1.038	1.046	1.055	1.056	1.057	1.064	1.065	1.068	1.069	1.065	1.071
1.55	1.007	1.009	1.017	1.026	1.036	1.046	1.052	1.064	1.072	1.078	1.082	1.093	1.093	1.099	1.110	1.106	1.119
1.6	1.008	1.009	1.019	1.028	1.043	1.054	1.063	1.077	1.085	1.091	1.101	1.112	1.117	1.126	1.395	1.142	1.152
1.65	1.008	1.010	1.020	1.028	1.048	1.059	1.070	1.086	1.093	1.102	1.113	1.124	1.133	1.145	1.160	1.168	1.184
1.7	1.008	1.010	1.020	1.027	1.050	1.062	1.075	1.090	1.098	1.108	1.119	1.130	1.142	1.154	1.171	1.186	1.207
1.75	1.007	1.010	1.019	1.025	1.049	1.063	1.076	1.091	1.098	1.107	1.120	1.130	1.146	1.156	1.175	1.192	1.212
1.8	1.007	1.010	1.018	1.023	1.045	1.061	1.074	1.087	1.095	1.104	1.115	1.128	1.142	1.152	1.174	1.190	1.210
1.85	1.006	1.009	1.017	1.020	1.040	1.055	1.067	1.080	1.088	1.097	1.104	1.120	1.130	1.142	1.161	1.175	1.195
1.9	1.006	1.008	1.016	1.018	1.034	1.047	1.059	1.070	1.077	1.086	1.091	1.106	1.119	1.126	1.140	1.152	1.172
1.95	1.005	1.007	1.014	1.016	1.028	1.039	1.051	1.059	1.065	1.075	1.077	1.090	1.097	1.108	1.119	1.129	1.145
2.0	1.005	1.006	1.012	1.014	1.022	1.031	1.042	1.048	1.052	1.062	1.063	1.074	1.079	1.087	1.096	1.105	1.117
2.05	1.004	1.005	1.009	1.011	1.016	1.024	1.033	1.036	1.040	1.047	1.047	1.056	1.060	1.065	1.072	1.078	1.087
2.1	1.004	1.004	1.007	1.009	1.010	1.016	1.024	1.024	1.027	1.034	1.032	1.040	1.043	1.043	1.049	1.053	1.056
2.15	1.003	1.003	1.005	1.006	1.004	1.009	1.013	1.013	1.015	1.019	1.016	1.024	1.024	1.025	1.026	1.027	1.031
2.2	1.002	1.003	1.003	1.003	0.998	1.001	1.004	1.002	1.004	1.006	1.003	1.007	1.007	1.005	1.007	1.006	1.003
2.25	1.002	1.002	1.001	1.001	0.992	0.994	0.992	0.990	0.992	0.994	0.998	0.991	0.989	0.987	0.988	0.983	0.976

TABLE I (Continued.)

Q	0.253	0.258	0.520	0.799	1.517	1.964	2.425	2.883	2.884	3.160	3.474	3.817	4.216	4.66	5.15	5.65	6.19
2.3	1.001	1.000	0.999	0.997	0.987	0.986	0.983	0.980	0.980	0.982	0.977	0.978	0.974	0.973	0.970	0.964	0.958
2.35	1.001	0.998	0.999	0.995	0.982	0.981	0.977	0.972	0.973	0.972	0.967	0.968	0.963	0.962	0.956	0.948	0.943
2.4	1.000	0.998	0.996	0.992	0.979	0.978	0.971	0.965	0.966	0.965	0.962	0.959	0.953	0.949	0.945	0.936	0.931
2.45	1.000	0.997	0.995	0.990	0.977	0.975	0.968	0.961	0.962	0.960	0.956	0.953	0.947	0.942	0.937	0.927	0.922
2.5	1.000	0.996	0.994	0.989	0.975	0.972	0.966	0.959	0.960	0.958	0.954	0.949	0.943	0.938	0.933	0.922	0.916
2.55	1.000	0.995	0.995	0.989	0.975	0.971	0.965	0.959	0.960	0.958	0.952	0.947	0.942	0.937	0.931	0.920	0.914
2.6	1.000	0.995	0.995	0.989	0.977	0.971	0.966	0.960	0.961	0.960	0.952	0.947	0.941	0.938	0.932	0.922	0.915
2.65	1.000	0.995	0.996	0.990	0.979	0.972	0.967	0.962	0.963	0.962	0.954	0.949	0.943	0.940	0.934	0.926	0.917
2.7	1.000	0.995	0.996	0.991	0.981	0.975	0.970	0.965	0.966	0.965	0.958	0.952	0.946	0.943	0.938	0.929	0.922
2.75	1.000	0.994	0.998	0.992	0.982	0.978	0.973	0.968	0.969	0.969	0.961	0.957	0.951	0.947	0.943	0.935	0.929
2.8	1.000	0.994	0.999	0.994	...	0.983	0.977	0.972	0.974	0.974	0.966	0.962	0.957	0.952	0.950	0.943	0.938
2.85	1.000	0.994	1.000	0.995	...	0.987	0.983	0.977	0.979	0.979	0.971	0.969	0.965	0.960	0.958	0.952	0.948
2.9	1.000	0.994	1.000	0.996	...	0.991	0.988	0.983	0.984	0.985	0.976	0.976	0.972	0.968	0.966	0.961	0.959
2.95	1.000	0.995	1.001	0.998	...	0.995	0.993	0.988	0.988	0.991	0.982	0.983	0.980	0.978	0.976	0.972	0.969
3.0	1.000	0.995	1.002	0.999	...	0.999	0.997	0.994	0.993	0.998	0.989	0.989	0.989	0.986	0.987	0.983	0.982
3.05	1.000	0.996	1.002	1.000	...	1.003	1.001	0.999	0.999	1.003	0.997	0.998	0.998	0.995	0.996	0.995	0.995
3.1	1.000	0.996	1.003	1.001	...	1.006	1.005	1.004	1.005	1.008	1.004	1.005	1.005	1.004	1.005	1.005	1.005
3.15	1.000	0.997	1.003	1.002	...	1.009	1.009	1.008	1.009	1.013	1.009	1.011	1.012	1.011	1.012	1.015	1.015
3.2	1.001	0.998	1.003	1.003	...	1.011	1.012	1.013	1.013	1.017	1.015	1.016	1.018	1.018	1.019	1.023	1.024
3.25	1.001	0.998	1.003	1.004	...	1.014	1.015	1.016	1.016	1.020	1.019	1.022	1.023	1.026	1.026	1.031	1.032
3.3	1.001	0.999	1.003	1.004	...	1.016	1.016	1.018	1.018	1.022	1.023	1.024	1.027	1.030	1.031	1.036	1.038
3.35	1.001	1.001	1.003	1.005	...	1.016	1.017	1.020	1.019	1.022	1.024	1.026	1.029	1.034	1.034	1.039	1.041
3.4	1.002	1.002	1.003	1.005	...	1.016	1.018	1.021	1.020	1.021	1.025	1.027	1.030	1.035	1.036	1.041	1.043
3.45	1.002	1.002	1.002	1.004	...	1.016	1.018	1.022	1.021	1.021	1.024	1.027	1.031	1.034	1.036	1.042	1.043
3.5	1.001	1.003	1.002	1.004	...	1.015	1.018	1.021	1.021	1.019	1.023	1.027	1.031	1.032	1.035	1.041	1.042
3.55	1.001	1.004	1.001	1.003	...	1.014	1.016	1.019	1.020	1.016	1.021	1.025	1.029	1.029	1.033	1.039	1.038
3.6	1.000	1.004	1.000	1.003	...	1.013	1.014	1.017	1.018	1.013	1.019	1.021	1.026	1.025	1.029	1.035	1.034
3.65	0.999	1.004	0.999	1.002	...	1.011	1.012	1.015	1.015	1.010	1.015	1.017	1.022	1.020	1.025	1.030	1.029
3.7	0.999	1.003	0.998	1.001	...	1.009	1.010	1.012	1.012	1.007	1.012	1.013	1.016	1.016	1.020	1.025	1.024
3.75	0.998	1.003	0.997	1.000	...	1.008	1.007	1.010	1.008	1.003	1.008	1.008	1.010	1.011	1.015	1.018	1.017
3.8	0.997	1.002	0.996	0.999	...	1.006	1.004	1.007	1.005	0.999	1.003	1.004	1.005	1.007	1.009	1.013	1.004
3.85	0.996	1.002	0.995	0.998	...	1.004	1.002	1.003	1.002	0.995	0.998	1.000	1.000	1.001	1.004	1.006	1.004
3.9	0.995	1.001	0.994	0.997	...	1.002	0.999	0.999	0.997	0.990	0.994	0.996	0.996	0.996	0.998	1.000	0.997
3.95	0.994	1.001	0.992	0.995	...	1.000	0.997	0.996	0.994	0.988	0.991	0.992	0.992	0.989	0.993	0.993	0.989
4.0	0.993	1.001	0.991	0.993	...	0.998	0.994	0.992	0.995	0.986	0.987	0.988	0.989	0.985	0.987	0.987	0.982

would view the sample. A run consisted of moving the detectors in angular steps of 0.5° from the minimum angle to the maximum angle and back. Typically 3×10^4 counts were recorded at each angle by each detector, for a total of 1.5×10^5 counts per angle. After completion of these measurements the pressure was changed to a new value and the procedure repeated. The list of 17 densities covered is given in Table I. In a typical case the krypton nuclei absorbed about one-third of the incident beam.

In addition, runs were taken with the vessels empty, with the vanadium samples, with no sample present, and with cadmium cylinders as samples. Finally, runs were taken periodically with cadmium covering the primary beam.

The beam profile was determined by measuring the variation in the scattered intensity (at a constant angle) from a vertical thin nylon wire as it was moved to different positions relative to the center. The location of the beam center relative to the sample was determined to 0.5 mm (a requirement for absorbing samples when the incident beam is smaller than the sample diameter). For vessel I there was a displacement of the beam relative to the sample center by 3.9 mm, while for all other cases the centers coincided. These data are required to calculate the absorption factors (see Sec. III).

III. DATA REDUCTION

The inelastic scattering correction is known as the Placzek[9] correction $P(\theta)$. For both krypton and vanadium it was calculated using the constant detector efficiency formula (since the efficiency for the incident wavelength is 94% for bank I and 78% for bank II):

$$P(\theta) = (m_n/M)[kT/2E_0 - 2(1 - \cos\theta)] + O(m_n/M)^2 ,$$
(7)

where θ is the scattering angle,[10] m_n and M are the neutron and atomic masses respectively, and E_0 is the energy of the primary neutrons. This correction ranges from 0.011 at $\theta = 0°$ to -0.017 at $\theta = 100°$ for krypton and is 65% larger for vanadium. The inclusion of the counter efficiency (using the manufacturer's specifications) was investigated and leads to a change varying from zero at 0° to a maximum at 90° of -0.5% of $S(Q)$. However, this is an upper limit, since the wall effect of the detectors will reduce their variation of efficiency with energy.

Adding this term to the right-hand side of Eq. (6) leads to the formula for the differential (single) scattering cross section per atom $d\sigma/d\Omega$, i.e.,

$$\frac{d\sigma}{d\Omega} = \frac{1}{4\pi}\{\sigma^{\mathrm{coh}}[S(\theta) - 1] + \sigma^{\mathrm{tot}}[1 + P(\theta)]\} ,$$
(8)

where q and θ are related by $q = (4\pi\sin\frac{1}{2}\theta)/\lambda$ and λ is the neutron wavelength.

The intensity $I'_{sc}(\theta)$ per unit of flux scattered by a sample (s) and container (c) having N_s and N_c atoms respectively in the beam is

$$K(\theta)[I'_{sc}(\theta) - B_{sc}]$$

$$= N_s A_{s,sc}(\theta)\left(\frac{d\sigma}{d\Omega}\right)_s + N_c A_{c,sc}(\theta)\left(\frac{d\sigma}{d\Omega}\right)_c$$

$$+ \frac{1}{4\pi}[N_s A_{s,sc}(\theta)\sigma_s + N_c A_{c,sc}\sigma_c]\Delta_{sc} ,$$
(9)

where $K(\theta)$ is the ratio of neutrons scattered per steradian to neutrons detected at angle θ, B_{sc} is the experimental background, and $A_{s,sc}(\theta)$ and $A_{c,sc}(\theta)$ are the absorption factors. Δ_{sc} is the ratio of multiple to single scattering and σ_s and σ_c are the total scattering cross sections per atom of the sample and container.

The absorption factors $A_{s,sc}$, $A_{c,sc}$, and $A_{c,c}$ were evaluated by numerical integration as described by Kendig and Pings,[11] where, e.g., $A_{s,sc}$ is the absorption factor for scattering from the sample with absorption in the sample plus vessel. In order to calculate[12] the angular variation in the absorption factors to the required precision, the actual beam profile with width less than the sample diameter and centers offset was used in the integrations.

We calculated the ratio of second to first scattering δ_p using numerical integration[12] for concentric cylinders with the beam plus sample geometry. Then δ was used to calculate the total multiple scattering from[12,13]

$$\Delta(\theta) = \frac{\delta_p(\theta)}{\delta(\theta)}\left(\frac{e^{-2\delta(\theta)} - 1}{2\delta(\theta)} - 1\right) ,$$
(10)

where $\delta_p(\theta)$ is the ratio of second to first scattering using the incident beam profile and sample geometry and $\delta(\theta)$ is the ratio of first to second scattering, assuming the sample and vessel are completely immersed in a uniform incident beam (which applies to the higher-order scatterings). Fortunately, Δ_{sc} is almost independent of angle and ranges, for example, from 0.036 for $\rho = 0.25$ to 0.100 for $\rho = 6.19$; $\Delta_c(\theta)$ was 0.036 for vessel II and 0.045 for vessel I. The difference between the centers of the beam and vessel I necessitated an additional small angular-dependent correction.

The coherent and total scattering cross sections vary with angle for krypton due to the neutron-electron interaction[14] and should be written as $\sigma_s E(\theta)$, where

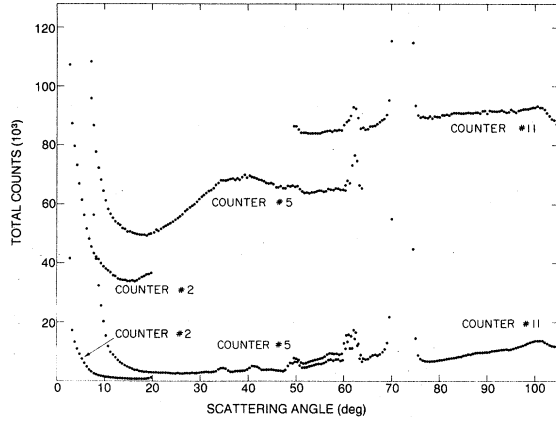$$E(\theta) = 1 + 8\pi b_e b_n \bar{z} f(\theta)/\sigma_s ,$$
(11)

FIG. 2. Raw data obtained from krypton at a density of 2.88. The upper three curves were obtained from the sample plus vessel II and the lower curve from empty vessel II.

where σ_s is the nuclear cross section, b_e is the electronic scattering length, b_n is the nuclear scattering length, z is the number of electrons, and $f(\theta)$ is the x-ray form factor. The quantity $E(\theta)$ increases the krypton cross sections by 0.4% at $\theta = 100°$ relative to their values at the origin.

Another correction needed to account for scattering from air in the neutron shielding was handled implicitly through the cross sections. A simple calculation, assuming isotropic scattering from air, showed that ~1.5% of the neutrons detected by each detector had been deflected from their original scattering angle by the air between the sample and the detectors. Since the effect of this is equivalent to increasing the incoherent background, it may be corrected for by increasing the ratio $\gamma = \sigma^{coh}/\sigma^{tot}$ by 1.5%.

The dead time of the monitor had been measured and the readings were corrected ($<1.5\%$) for changes in monitor counting rate due to the reactor power changing. An example of the raw data ob-

tained is in Fig. 2, which shows the measured intensity from the vessel plus krypton at a density of 2.88 and the intensity from the vessel alone for a single detector from each of the three kinds of run. The final results given later in this section have been obtained from five times the number of counts shown (since five detectors are summed in Sec. IV) for the intermediate- and large-angle measurements and twice the number of counts shown for the small-angle results. An effective number N of atoms in the beam was calculated by folding the beam profile with the distribution of material in the sample or container, each of which was assumed to be of uniform density, so that this integration involved the distribution of scattering volume alone. This step is not critical, however, since the final expression [(Eq. (16)] involves ratios of these quantities.

The background B_{sc} was determined from the equation

$$B_{sc} = [B_g(\theta) - B_{Cd}(\theta)]T_{sc} + B_{Cd}(\theta), \qquad (12)$$

where $B_g(\theta)$ and $B_{Cd}(\theta)$ are the intensities measured respectively without a sample in the incident beam and with a cadmium cylinder replacing the vessel; T_{sc} is the measured transmission of the incident beam through the sample and vessel. Although this expression is correct at small angles only, we have used it at larger angles, since $B_g(\theta) - B_{Cd}(\theta)$ was very small. Typically, B_{sc} was about 2% of I'_{sc}.

If we denote the intensity after subtraction of the background by $I(\theta)$, then Eq. (9) can be evaluated for the vanadium, the vessels, and the vessels plus sample to give (subscripts v, c, and s stand for vanadium, container, and sample, respectively)

$$I_v(\theta) = \rho_v V_v A_{v, v}(\theta)\sigma_v^{inc}[1 + \rho_v(\theta) + \Delta_v(\theta)]/K(\theta), \qquad (13)$$

$$I_c(\theta) = \rho_c V_c A_{c, c}(\theta)\sigma_c^{tot}\{[S_c(\theta) - 1]\gamma_c + [1 + P_c(\theta) + \Delta_c(\theta)]\}/K(\theta), \qquad (14)$$

$$I_{sc}(\theta) = \rho_s V_s A_{s, sc}(\theta)\sigma_s^{tot}\{[S_s(\theta) - 1]\gamma_s + [1 + P_s(\theta) + \Delta_{sc}(\theta)]\}[E(\theta)/K(\theta)]$$

$$+ \rho_c V_c A_{s, sc}(\theta)\sigma_c^{tot}\{[S_c(\theta) - 1]\gamma_c + [1 + P_c(\theta) + \Delta_{sc}(\theta)]\}/K(\theta), \qquad (15)$$

where ρ is the density and V is the irradiated volume, and we have ignored the electronic contribution $E(\theta)$ for the vanadium and the container. [Note that in Eq. (15) the multiple scattering contribution, proportional to Δ_{sc} in Eq. (9), has been split into two parts.]

The factor $1/K(\theta)$ was evaluated for each detector from the vanadium data by Eq. (13), and

though different for each detector, it was found to be independent of angle for all detectors.

We then find readily from Eqs. (13)–(15) that

$$\left(I_{sc}(\theta) - I_c(\theta)\frac{A_{s, sc}(\theta)}{A_{cc}}\right)\frac{\rho_v V_v A_{v, v}\sigma_v^{inc}F_v(\theta)}{\rho_s V_s A_{s, sc}\sigma_s^{tot}E(\theta)F_{sc}(\theta)I_v(\theta)}$$

$$= a\left([S_s(\theta) - 1]\frac{\gamma}{F_{sc}(\theta)} + 1\right), \qquad (16)$$

where $F_v(\theta) = 1 + P_v(\theta) + \Delta_v(\theta)$ and

$$F_{sc}(\theta) = 1 + P_s(\theta) + \Delta_{sc}(\theta)$$

$$+ \frac{\rho_c V_c A_{c,sc}(\theta)\sigma_c^{tot}}{\rho_s V_s A_{s,sc}(\theta)\sigma_s^{tot}}[\Delta_{sc}(\theta) - \Delta_c(\theta)], \qquad (17)$$

and we note that experimental quantities such as volume always occur in ratios. A factor a has been included in (16) to cover the possibility of systematic errors in the factor on the first line of the equation.

IV. REDUCTION TO $S(q)$ AND ERROR ANALYSIS

We can now find $S_s(\theta)$ for every value of θ (which are slightly different for different detectors and typically are spaced in q by 0.02Å^{-1}). For convenience the quantity $\gamma[S_s'(\theta) - 1]/F_{sc}(\theta) + 1$ was used in the following calculations. A four-point Lagrangian interpolation for constant steps in q of 0.01Å^{-1} was used for the data from each detector, and then results from all similar detectors within a given run were averaged together. Smooth curves were drawn by "eye" through these results and values read off at 0.05-Å^{-1} steps in q to give data with a statistical fluctuation of 0.1 to 0.2%, depending on density. At this stage the results for each density consisted of averaged curves from the large and intermediate-angle runs, and two curves from the small-angle run, one each for the two types of detector. A comparison of these curves showed systematic differences of < 0.3%, which were removed by matching to the large-angle results. An exception to this were the results from the small-angle run (3-6°) with the masked-down detectors using vessel I, where differences up to 5% were observed; this was assumed to be a systematic error. Since the angular variation appeared to be the same, these small-angle results were normalized to the overlapping intermediate-angle results. (The significance of taking data with different sets of detectors and comparing them is that it can reveal some sources of error.)

The structure factor $S(q)$ can now be evaluated. However, the accumulation of errors in the cross sections, numbers of atoms in the beam, etc., lead to a systematic error which may be several percent. Provided the angular dependence of all the corrections has been found properly, this accumulated error is mainly contained in the multiplicative constant a introduced in Eq. (16). This constant was found by comparing the data to the results of virial-series calculations based on the krypton pair potential[15] for values of q between 2.3 and 3.7Å^{-1}. In this range, $S(q)$ is not very sensitive to the details of the potentials and $S(q) - 1$ is small, having a maximum value of only 0.045 at $q = 3.45\text{Å}^{-1}$ for $\rho = 6.2$, so that calibrations to bet-
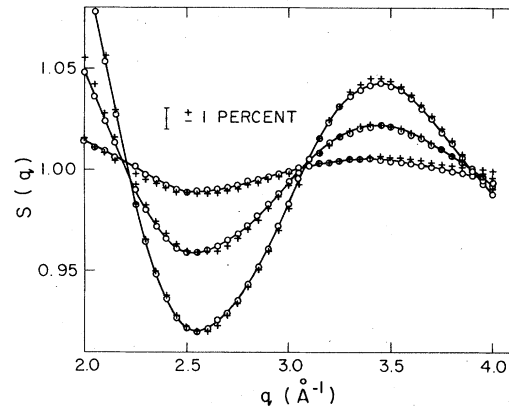

FIG. 3. Results of calibration for densities 0.80, 2.88,[17] and 5.65 in the momentum-transfer range 2 Å^{-1}– 4 Å^{-1}. Open circles show experimental data and crosses a calculation using the virial series.[15]

ter than 1% can be made. The main criterion employed was that the ratio of the minimum value to the maximum value over this range should be the same for the measured and calculated values, to 0.1% in $S(q)$.

Examples of the results of the calibration are in Fig. 3, which shows the calibrated measured structure factors for the densities[17] 2.88 and 5.65 along with the corresponding calculated structure factors in the range $q = 2.0 - 4.0\text{Å}^{-1}$. The value of the multiplicative constant varied systematically with density for the results obtained with vessel I, ranging from 1.008 at $\rho = 2.88$ to 0.999 at $\rho = 6.19$, with a scatter of ~0.15%. The value for vessel II varied smoothly (~0.2%) from 0.990 for $\rho = 0.5$ to 0.983 at $\rho = 2.5$, with an exceptional value of 0.987 for $\rho = 2.883$. The differences between the values for the two vessels are probably due to errors in the number of atoms in the beam. The observed variation with density is consistent with the uncertainty in the absorption cross section for krypton.

Since $F_{sc}(\theta)$ [(Eq. (17)] varies by only a small amount (e.g., for $\rho = 2.883$ it varied from 1.10 at 0° to 1.07 at 100°), the remaining error lies in the cross section ratio γ. A survey of measured cross sections for krypton was made and the following "best values" were chosen (σ_s and σ^{coh} in barns):

$$\sigma_s = 7.54, \quad \sigma^{coh} = 0.20, \quad \gamma = 0.976 \pm 0.022.$$

The error in γ could change the amplitude of $S(q) - 1$ and lead to a discrepancy in the level of $g(r)$ for $r < \sigma$, when the data are Fourier transformed. This will be considered later.

The structure factors obtained in this way are listed in Table I, and examples are shown in Fig. 4. Estimating the precision of the measured $S(q)$ is difficult, since most of the error is systematic. In order to obtain some estimate, we Fourier-
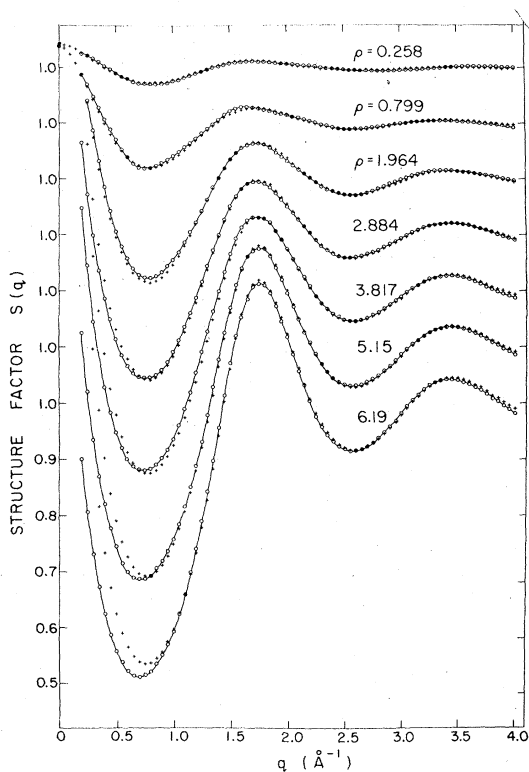
FIG. 4. Seven examples of measured structure factors of krypton at 297 K and densities shown.[17] Open circles and lines show experimental results; crosses (calculated for q values corresponding to the circles) show results predicted by the three-term virial expansion[15] using pair forces only.

transformed the measured $S(q)$; to extend the data from $q = 4\text{Å}^{-1}$ to higher values, we have used the virial series.[15] Only the leading term is significant in this range and it may be calculated from the pair potential alone. Thus we obtain the pair distribution function $g(r)$, and examples[17] are shown in Fig. 5. We inspect the region $r < \sigma$ (where σ is an atomic diameter) where $g(r)$ should be approximately zero. Any structure in this range must be due to errors in the structure factor from which it was obtained. This small r structure was deleted and the result was transformed back to $S(q)$, and the differences between these results and those of Table I were as follows.

For $\rho = 0.253$ Table I is higher by up to 0.9% in the range $q = 0.55 - 1.2\text{Å}^{-1}$, for $\rho = 0.520$ by up to 1.3% for $q = 0.25 - 1.4\text{Å}^{-1}$, and for both densities by 0.4% over the rest of the q range. The results for $\rho = 0.258$ were in agreement to ~0.3% for all q values, with discrepancies up to 0.5% for a few points near $q = 0.65$ and 2.9Å^{-1}. For $\rho = 0.799$ the agreement was ~0.5% or better, with the exception of $q = 0.3 - 0.5$, where there were discrepancies of up to 0.8%. For densities $1.52 - 2.88$ the differences were $\sim \pm 0.5\%$ for $q \geqslant 1.0\text{Å}^{-1}$; the values in Table I were higher by up to ~1% in the range $0.5 \leqslant q < 1.0 \text{ Å}^{-1}$ and up to ~2% at the smallest q values. For $\rho = 2.88 - 5.15$ there was agreement to $\sim \pm 0.5\%$ or better for $q > 0.4\text{Å}^{-1}$. Similar results were found for $q < 0.4\text{Å}^{-1}$; however, the statistical error in this range is of the order of 1%. For
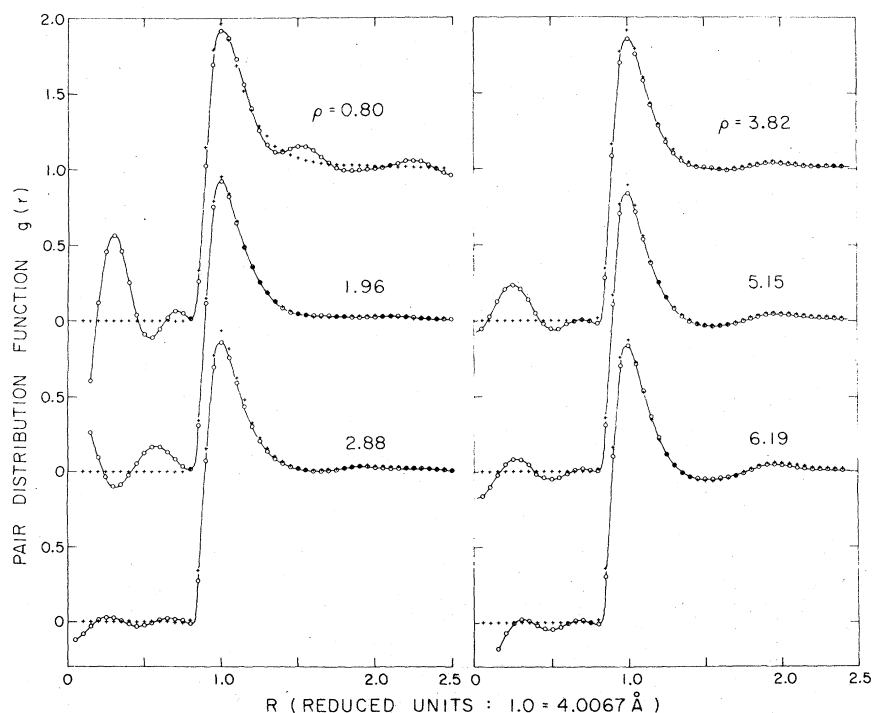

FIG. 5. Pair distribution functions for krypton for six highest densities shown in Fig. 4. Open circles and lines show pair distribution functions obtained by Fourier-transforming the experimental results. Crosses show results predicted by virial expansion using pair forces only. Note that a 0.5% error in $S(q)$ becomes magnified at low densities in this representation.

two cases, $\rho = 3.16$ and 3.82, a few values at the first peak ($q = 1.75 \text{Å}^{-1}$) were too high by 0.65% and 0.75%, respectively. For the two highest densities Table I appeared to be lower in the range $q \lesssim 1.2 \text{Å}^{-1}$ by $\lesssim 1.3\%$ for $\rho = 5.65$ and $\lesssim 0.9\%$ for $\rho = 6.19$, and for $q > 1.2 \text{Å}^{-1}$ the differences were $\sim \pm 0.5\%$. Consequently, this test confirms that the measured $S(q)$ functions are reliable to better than 1% for most of the data listed. In addition, Fig. 5 (especially[17] $\rho = 2.884$) showed that for $r < \sigma$ the level of $g(r)$ is correct, thus confirming the choice of γ.

At the lowest density the virial expansion using the pair potential should give an accurate estimate for $S(q)$, and this calculation agreed with our data within the stated experimental error (Fig. 4). Comparison of the two densities, $\rho = 2.883$ and 2.884, for which both vessels were used showed a maximum difference of 0.3% for $q \geqslant 2.1 \text{Å}^{-1}$ and an average difference of 0.1% in this range. For $0.8 \leqslant q \leqslant 2.05 \text{Å}^{-1}$ there were some differences slightly greater than 0.5%. These two comparisons confirm that our precision is better than 1%.

Further analysis of these discrepancies could be used to increase the precision, but we have chosen not to do so, since the experimental precision is good enough for our present purpose.

V. DISCUSSION

In Figs. 4 and 5, in addition to the measured structure factors and pair distribution functions, we have shown for comparison the results from the virial calculations for a number of densities. At the lowest densities there are no significant differences between the virial expansion and the measurements; at the higher densities, however, there are small differences larger than the errors. We attribute these differences mostly to many-body forces, the dominant of these being the three-body force.

In addition, we have compared the calculated and measured structure factors by plotting the data at each q as a function of density. There was generally good agreement at low densities, but some small discrepancies were observed for $0.9 \leqslant q \leqslant 1.1 \text{Å}^{-1}$, $1.8 \leqslant q \leqslant 2.0 \text{Å}^{-1}$, and $2.6 \leqslant q \leqslant 2.9 \text{Å}^{-1}$. (We ignore these small discrepancies in our discussion of the three-body term.) Since at low densities atoms interact only in pairs, this indicates that our results are in fairly good agreement with the pair potential of Barker et al.[2] As the density increases, the experimental and calculated values diverge, and the difference is sufficient to measure the three-body contribution.

It is known that the long-range triple-dipole force suppresses the peak of $g(r)$; this is also true of the measured many-body force, as is apparent in Fig. 5, where we have compared the results of the virial calculations (using pair forces only) for $g(r)$ to the pair distribution functions obtained by transforming our data. Also this figure confirms our comments in the Introduction concerning the range over which the measurements are sensitive to the interatomic potentials. At the lower densities ($\lesssim 3.5$) our measurements are clearly sensitive to the form of the potential to at least one atomic diameter beyond the first peak in $g(r)$; at the higher densities the appearance of a prominent second peak in the pair distribution function indicated that geometric packing effects limit the range. The initial rise of $g(r)$ from $r = 0.8$ to 0.9 is governed by the repulsive part of the pair potential. Comparison of the experimental and calculated points shows experimental results consistently below the calculated points by an amount which is approximately constant. This indicates a minor discrepancy between our experiment and the pair potential of Barker et al.; the zero of this potential would have to be shifted from $r = 3.573$ to 3.594Å to agree with our results (Karnicky et al.[5] measured 3.389 for argon compared to a prediction of 3.361). The height of the principal peak of $g(r)$ as a function of density is shown in Fig. 6, where experimental results are compared to the Monte Carlo calculations[18] and to virial computations.[15] For the 297 K isotherm the peak height decreases with increasing density until $\rho \simeq 6.0$. The suppression of the peak height due to the three-body potential is clearly demonstrated in this graph, particularly in the range $\rho \sim 2$–4.5.

In order to extract the term $C_2(q, T)$ in Eq. (4) from the data, we calculated the direct correlation function $c(q)$ from the structure factors given in Table I. In Fig. 7 we have plotted the experimental $c(q)$ as a function of density for values of q from zero (from PVT data) to 2.5Å^{-1} in steps of 0.1Å^{-1} for the data points for which the "error" in the structure factor revealed by our tests was $\sim \pm 0.5\%$ or less. The solid lines on this graph were com-
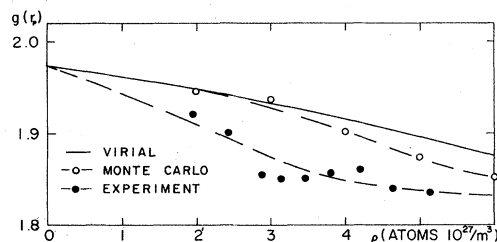

FIG. 6. Principal peak height for krypton gas at 297 K. Solid line is a virial calculation and open circles are Monte Carlo results (Ref. 18) based on the pair potential. Solid circles are experimental results. Dashed lines serve as a guide to the eye.
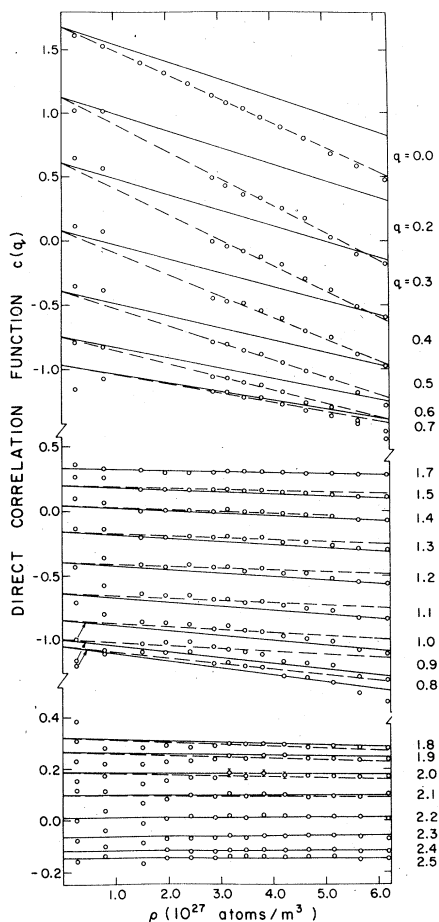
FIG. 7. Direct correlation function as a function of
density. Solid lines were calculated from the pair po-
tential. The difference between solid and dashed lines,
drawn through the lower–density experimental points, is
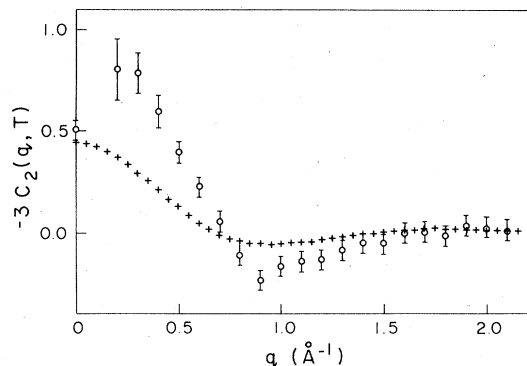due almost entirely to the three-body force.

FIG. 8. $C_2(q,T)$ obtained from the difference
$C(q,T)_{\text{pair}} - C(q,T)_{\text{exp}}$ shown in Fig. 7. Experimental
values are shown as open circles with error bars; the
latter were attained by estimating a range of acceptable
slopes for data of Fig. 7. Crosses are calculated from
Axilrod-Teller three-body potential.

puted from the known pair potential where the in-
tercept is $-2B(q,T)$ and the slope is $-3C_1(q,T)$.
As can be seen from this graph, there seems to be
no serious disagreement between the calculated
values of $-2B(q,T)$ and the intercepts of the data
extrapolated to $\rho = 0$ [although in many cases this
is not a satisfactory test for the correctness of
$B(q,T)$]. It is also clear that the data lie along
straight lines within our errors. The dashed lines
were drawn through these points and the calculated
values of $-2B_2(q,T)$. Thus the slopes of the dashed
lines are best estimates of $-3[C_1(q,T)+C_2(q,T)]$.

The result at $q = 0$ is well known from PVT data.
The remaining results, however, are new and re-
present the first direct experimental measurement
of the functional dependence of the three-body-po-
tential contribution. The difference between the
solid and dashed lines in proportional to $C_2(q,T)$.

As q increases, this contribution initially in-
creases, then falls to its original value at about
$q = 0.5\text{Å}^{-1}$ and continues to decrease, so that it is
negative from approximately $q = 0.8$ to 1.5Å^{-1}.
Beyond $q = 2.1\text{Å}^{-1}$ its contribution is comparable
to our errors, and beyond 3.5Å^{-1} both $C_1(q,T)$ and
$C_2(q,T)$ make a negligible contribution. Hence for
$q > 3.5\text{Å}^{-1}$, $S(q) - 1$ is given by $B(q,T)$ alone, as
assumed in our calibration procedure.

This functional dependence is shown quantitative-
ly in Fig. 8, where we have plotted $-3C_2(q,T)$,
the difference of the measured and calculated
slopes of Fig. 7, as a function of q. Also shown
on this graph is $-3C_2(q,T)$, calculated from the
triple-dipole potential,[2,7] which gives the correct
third virial coefficient in the pressure expansion.
It is clear that this term does not agree with the
measured $C_2(q,T)$. The amplitude of the latter is
approximately twice that of the calculated term,
which may indicate that it is approximately twice
the repulsive strength. The initial rise in the
measured $C_2(q,T)$ indicates a weakly attractive
part in the three-body potential for $2 \leqslant r \leqslant 4\text{Å}$.
This is consistent with an increased repulsion at
smaller r, since the two effects combine to give
the correct third virial coefficient. The Axilrod-
Teller form would take over at larger r. How-
ever, we must inject a note of caution, since, for
example, the attraction for $r \gtrsim 2.0$ might be re-
moved by modifying the pair potential, because
the interpretation of our results depends on the
accuracy of $B(q,T)$. Thus experiments of even
higher precision at low ρ would be desirable, since
they would enable $B(q,T)$ to be measured and
$C(q,T)$ to be extracted more reliably. This might
also entail measurements at other temperatures.

---

[1]S. A. Rice and P. Gray, *Statistical Mechanics of Simple Liquids* (Wiley, New York, 1965).

[2]J. A. Barker, R. O. Watts, J. K. Lee, T. P. Schafer, and Y. T. Lee, J. Chem. Phys. 61, 3081 (1974).

[3]R. A. Aziz, Mol. Phys. 38, 177 (1979).

[4]H.-P. Hansen and L. Verlet, Phys. Rev. 184, 151 (1969).

[5]J. F. Karnicky, H. H. Reamer, and C. J. Pings, J. Chem. Phys. 64, 4592 (1976).

[6]P. A. Egelstaff, R. K. Hawkins, L. Hahn, and A. Teitsma (unpublished).

[7]L. J. Groome, Ph.D. thesis, University of Florida, 1977 (unpublished).

[8]N. J. Trappeniers, T. Wassenaar, and G. J. Wolkers, Physica (Utrecht) 32, 1503 (1966).

[9]G. Placzek, Phys. Rev. 86, 377 (1952).

[10]Because high counters are used, the mean angle is the angle between the incident beam direction and a line joining the sample center to a point one-quarter counter height above the scattering plane.

[11]A. P. Kendig and C. J. Pings, J. Appl. Phys. 36, 1692 (1965).

[12]A. K. Soper and P. A. Egelstaff (unpublished).

[13]V. F. Sears, Adv. Phys. 24, 1 (1975).

[14]V. E. Krohn and G. R. Ringo, Phys. Rev. 148, 1303 (1966).

[15]Two virial calculations were available to us. The data of Groome[7] for the Barker[2] $u(r)$ can be used for the first three terms in the series

$$g(r) = g_0(r) + \rho g_1(r) + \rho^2 g_2(r) + \cdots$$

and Fourier transformed to $S(q)$. In addition, Wertheim[16] has calculated $B(q,T)$ and $C_1(q,T)$ for the Barker $u(r)$ and these data can be used in the equation

$$S(q) = 1 - 2\rho B(q,T) + \rho^2[4B^2(q,T) + 3C_1(q,T)] + O(\rho^3).$$

These truncated series are sufficient to give accurate results at low densities for all q and at our highest densities for high q. It should be noted that the number of terms needed is in general a strong function of q.

[16]M. S. Wertheim (private communication).

[17]The result for the two experiments at $\rho = 2.88$ in Table I have been averaged for $q > 0.8$ Å^{-1} and the results for vessel I were used for $q < 0.8$ Å^{-1}, since they were more accurate. The Fourier-transform test of these averaged data showed discrepancies of $\lesssim 0.3\%$.

[18]P. A. Egelstaff, A. Teitsma, R. McPherson, and S. S. Wang (unpublished).